Proceedings of the 17th World Congress
The International Federation of Automatic Control
Seoul, Korea, July 6-11, 2008

Dynamics of Integrated Silicon Micro-heaters

Abu Sebastian * **Dorothea Wiesmann** *

* *IBM Zurich Research Laboratory, 8803 Rüschlikon, Switzerland*

Abstract: Micro-cantilevers with integrated heaters serve as powerful tools for investigation and manipulation at the nanometer scale. They can be used to locally heat surfaces. They can also serve as low-cost, highly integrable topography sensors, and find application as position sensors for nanopositioning applications. In this paper we present a tractable feedback model that captures the thermo-electric dynamics of these micro-heaters. A systems approach is preferred over a modeling approach based on the underlying physical mechanisms. Experimental results on the write/read heaters and the thermal position sensors from a probe-based data-storage device are presented.

1. INTRODUCTION

Heated probes find applications in areas ranging from micro-thermal analysis to the study of heat transport at the nanoscale (see Pollock and Hammiche [2001], Cahill et al. [2003]). They can be used to generate fast heat pulses and to heat surfaces with high spacial resolution. They can also serve as topography sensors. Both these capabilities are utilized in the scanning-probe-based data-storage concept being pursued by IBM, where an array of micro-cantilevers with integrated micro-heaters is used to write and read back information on thin polymer films (see Eleftheriou et al. [2003]). The schematic of one such micro-fabricated silicon cantilever is shown in Figure 1. Parts of the cantilever are designed to be heaters having an area of approximately 4 μm $\times$ 4 μm heaters are produced by varying the doping levels and can be heated by applying an electrical current through the cantilever legs and the heater. Constant voltage excitation is typically employed.

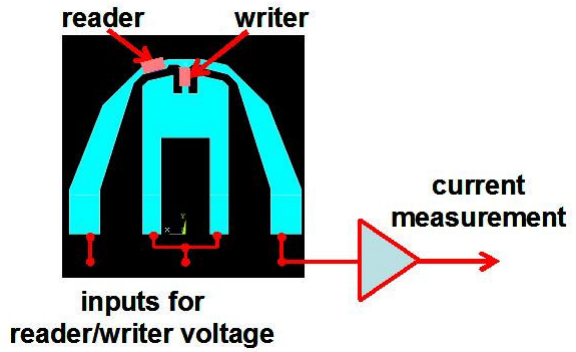

Fig. 1. Schematic of a micro-fabricated silicon cantilever with integrated read and write heating elements.

For both the read and the write micro-heater, heat transportation is primarily through the air gap between the heater and the sample and through the cantilever legs. For the write heaters, the tip is manufactured to sit directly underneath the heater area. A small fraction of the heat gets transported through the tip-surface contact into the sample. The read heaters are typically heated to lesser temperatures, and the subsequent topography sensing is based on the following two premises. (1) The heat conduction through air depends on the distance of the sensor from the substrate. (2) The resistance of the heater is a strong function of the temperature. As the cantilever tip follows the topographical variations, the distance of the read heater from the substrate gets modulated by the topographical variations. This translates to a difference in cooling. The subsequent change in the electrical resistance is measured as a change in the current in the case of constant voltage excitation.

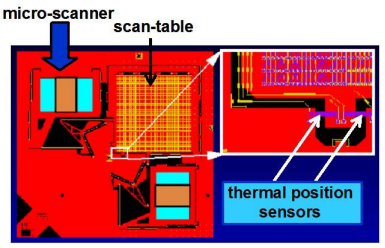

Fig. 2. Picture of the micro-scanner and the thermal position sensors.

Micro-heaters also find application as position sensors in nanopositioning applications (see Lantz et al. [2005]). In probe-based data storage, a micro-scanner as shown in Figure 2 is used to position the polymer medium underneath the array of micro-cantilevers. The scan table can be displaced in the X/Y directions in the plane of the silicon wafer. Two pairs of thermal position sensors are used to provide position information of the micro-scanner. These sensors are fabricated on the cantilever-array chip and are positioned directly above the scan table. The sensors consist of micro-heaters made from moderately doped silicon (Fig. 2). Displacement of the scan table translates into a change in the overlap of the micro-heaters with the scan table. This results in a change in the cooling and thus a change in their electrical resistance. By driving the sensors with a constant voltage, these changes in resistance can be detected by measuring the resulting current.

In view of the numerous applications, there is a significant interest in understanding the dynamics of micro-heaters (see Dürig [2005], Wiesmann and Sebastian [2006], Park et al. [2007]). Owing to the seemingly complicated dynamics, the interplay between thermal and electrical responses and finite-size effects, numerical simulations are widely preferred over analytical approaches for investigating the operation of micro-heaters. One approach to analytical modeling is to start from physical principles governing the heat transfer and the electrical characteristics of doped silicon and then arrive at dynamical relations between the signals of interest (see Dürig [2005]). The closeness of the model to physically interesting variables make this approach particularly interesting. However, the intricate design of the micro-heaters, fabrication tolerances, and finite

size effects make the direct application of this approach less practical. In this paper we present a systems approach to the modeling of these micro-heaters. The tractability and simplicity of the model and the ease of identification make this approach very powerful.

2. MODELING AND IDENTIFICATION

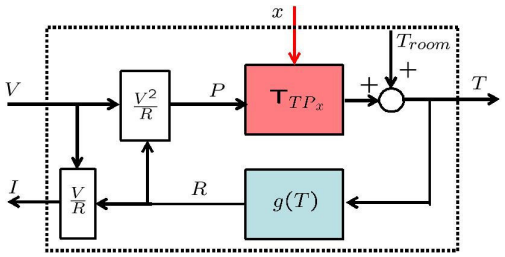

Fig. 3. The model of the micro-heater derived from a systems perspective

The systems-inspired model of the micro-heater is described in Figure 3. The main components are a linear operator relating power with temperature and a nonlinear operator relating the temperature with electrical resistance. The linear operator relating the input power to the temperature is modeled by $\mathbf{T}_{TP_x}$. $\mathbf{T}_{TP_x}$ captures the dynamics of thermal conduction as a function of the power dissipated in the heating elements when the heater sample separation equals x. In the case of the thermal position sensors, x corresponds to the position of the micro-scanner that determines the overlap between the micro-heater and the scan table. $\mathbf{T}_{TP_x}$ captures the thermal system for that particular x and $g(.)$ models the memoryless nonlinear relationship between temperature and the electrical resistance. $g(.)$ is typically a bell-shaped curve with the resistance value reaching a maximum at a certain temperature $T_{\max}$. Below $T_{\max}$, the resistance increases with temperature because of a corresponding decrease of the mobility of the majority carriers. However, above $T_{\max}$, the resistance becomes smaller with increasing temperature owing to the predominance of the thermally activated increase of the carrier density. The signal that is measured experimentally is the current, i.e. the input voltage divided by the resistance of the heater.

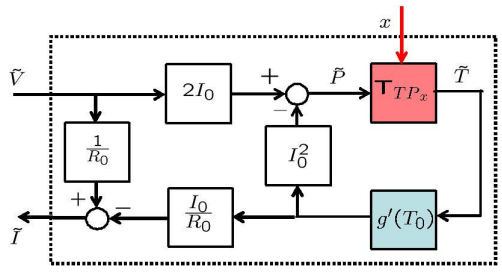

Fig. 4. Linearized version of the model.

For small-signal analysis, we can linearize the various nonlinear blocks about an operating point using the Taylor series expansion, and obtain the linear model shown in Figure 4, where $V = V_0 + \tilde{V}$, $I = I_0 + \tilde{I}$, $R = R_0 + \tilde{R}$, $T = T_0 + \tilde{T}$, and $P = P_0 + \tilde{P}$. Such a linear model facilitates the calculation of transfer functions relating the signals of interest. One of them is the transfer function relating the current fluctuation with the input voltage fluctuation at a certain heater-sample separation x and a certain operating voltage, denoted by $\mathbf{T}_{\tilde{I}\tilde{V}_x}$. The importance of this transfer function stems from the fact that it is easier to measure experimentally and that it can be used to obtain $\mathbf{T}_{TP_x}$. From the linear model, $\mathbf{T}_{\tilde{I}\tilde{V}_x}$ is given by

$$\mathbf{T}_{\tilde{I}\tilde{V}_x} = \frac{1}{R_0}\left(\frac{1 - I_0^2 g'(T_0)\mathbf{T}_{TP_x}}{1 + I_0^2 g'(T_0)\mathbf{T}_{TP_x}}\right), \tag{1}$$

where $g'(T_0)$ denotes the slope of $g(.)$ at T_0. Note that the linear assumption for $\mathbf{T}_{\tilde{I}\tilde{V}_x}$ holds only for small fluctuations in voltage and current, whereas $\mathbf{T}_{TP_x}$ is assumed to be linear over the whole range of operating points. The transfer function, $\mathbf{T}_{TP_x}$ can be derived from $\mathbf{T}_{\tilde{I}\tilde{V}_x}$ using

$$\mathbf{T}_{TP_x} = \frac{1}{I_0^2 g'(T_0)}\left(\frac{1 - R_0\mathbf{T}_{\tilde{I}\tilde{V}_x}}{1 + R_0\mathbf{T}_{\tilde{I}\tilde{V}_x}}\right). \tag{2}$$

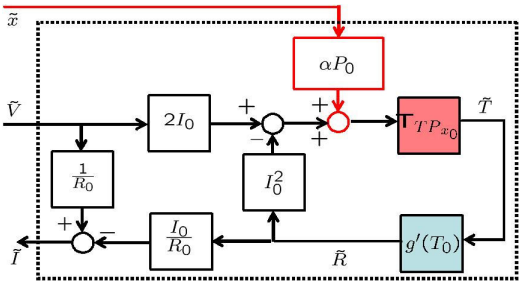

Fig. 5. The model for the micro-heater in which the perturbation of $\mathbf{T}_{TP_x}$ is cast as an input to the feedback system.

For the write heaters, the identification of the elements in the nonlinear model completely characterizes the large-signal behavior for a fixed heater-sample separation x. However, for the read heaters, the operator of interest is $\mathbf{T}_{\tilde{I}\tilde{x}_x}$ which relates the fluctuation in current to the fluctuation in heater-sample separation about an operating point of the heater-sample separation, x_0. The heater-sample separation, $\tilde{x}$, modifies the operator $\mathbf{T}_{TP_x}$. This perturbation of the thermal system is detected by monitoring the current fluctuations. Thermo-mechanical sensing can be viewed in the context of the general class of problems in which the perturbation of a linear time-invariant system is detected by monitoring signals within a feedback configuration it is part of. The efficiency (sensitivity) and speed (bandwidth) of detection of this change can be studied using linear transfer functions. For simplicity, one can assume that $\tilde{x}$ perturbs the gain of the operator $\mathbf{T}_{TP_x}$ alone. This is clearly an oversimplification and later on it will be shown that even the dynamic component of $\mathbf{T}_{TP_x}$ changes significantly with $\tilde{x}$. However, it can be shown that for the specific micro-heaters we are investigating, the gain perturbation is primarily responsible for sensing. So we persist with the assumption and let the dynamics of $\mathbf{T}_{TP_x}$ be described by

$$\mathbf{T}_{TP_x}(s) = K(x)\frac{b(s)}{a(s)}, \tag{3}$$

where $K(x)$ is the gain of $\mathbf{T}_{TP_x}$ as a function of the heater-sample separation, x, and $b(s)$ and $a(s)$ are polynomials of s. Then linearizing $\mathbf{T}_{TP_x}$ about x_0 gives

$$\mathbf{T}_{TP_x}(s) = K(x_0)\frac{b(s)}{a(s)} + K'(x_0)\frac{b(s)}{a(s)}\tilde{x}. \tag{4}$$

Hence under the assumption that only the gain of $\mathbf{T}_{TP_x}$ is modulated by $\tilde{x}$, $\tilde{x}$ enters the feedback loop as another input. The resulting system is depicted in Figure 5. The sensing transfer function is given by

$$\mathbf{T}_{\tilde{I}\tilde{x}_x} = \frac{K'(x)}{K(x)}\left(\frac{-I_0}{R_0}\frac{g'(T_0)P_0\mathbf{T}_{TP_x}}{1 + I_0^2 g'(T_0)\mathbf{T}_{TP_x}}\right). \tag{5}$$

Note that $\mathbf{T}_{TP_x}$ can be thought of as the "open-loop" transfer function. $\mathbf{T}_{\tilde{IV}_x}$ and $\mathbf{T}_{\tilde{I}\tilde{x}_x}$ can be thought of as the "closed-loop" transfer functions. It can also be seen that $\mathbf{T}_{\tilde{I}\tilde{x}_x}$ has a higher bandwidth than $\mathbf{T}_{TP_x}$. This is due to the inherent electrical feedback. Hence thermo-electric sensing is faster than the dynamics of the thermal system.

The first step in the identification process is the identification of $g(.)$. In a typical experiment, a ramp voltage signal is applied to the heater and the corresponding current is measured. From the voltage and current signals, the power vs. resistance map is obtained. From our modeling assumption, the relationship between power and temperature is linear. Moreover, $T_{\max}$ is known from the doping levels of the micro-heater. Using these two facts, the temperature vs. resistance map can be obtained.

The next step in the identification process is that of the LTI operator $\mathbf{T}_{TP_x}$. A DC voltage with a small-amplitude noise signal added on top is input to the heater. The corresponding current fluctuation is measured. The resistance fluctuation can be obtained from the voltage and current measurements. Using the identified relationship between temperature and resistance, $g(.)$, the temperature fluctuation can be obtained as $\tilde{T} = g^{-1}(R) - g^{-1}(R_0)$. The power fluctuation is measured as $\tilde{P} = VI - V_0 I_0$. From $\tilde{P}$ and $\tilde{T}$, the frequency response of $\mathbf{T}_{TP_x}$ can be obtained. A proper stable transfer function can be used to fit the experimentally measured frequency response. We call this method the direct method. An alternative approach to the identification of $\mathbf{T}_{TP_x}$ is to fit a stable transfer function to the frequency response obtained for $\mathbf{T}_{\tilde{IV}_x}$ and then to use the relationship given by Equation (2) to obtain $\mathbf{T}_{TP_x}$. We call this approach the indirect approach. Note that for this approach, the noise signal has to be small enough for $\mathbf{T}_{\tilde{IV}_x}$ to be sufficiently linear, whereas for the former approach the smallness of the noise signal is not very critical. In the subsequent sections both approaches will be employed for the identification of the thermal system $\mathbf{T}_{TP_x}$.

3. THE WRITE MICRO-HEATER

In this section we present the experimental identification of the write heater. We also demonstrate the generation of arbitrary temperature signals using the model identified.

3.1 Experimental identification

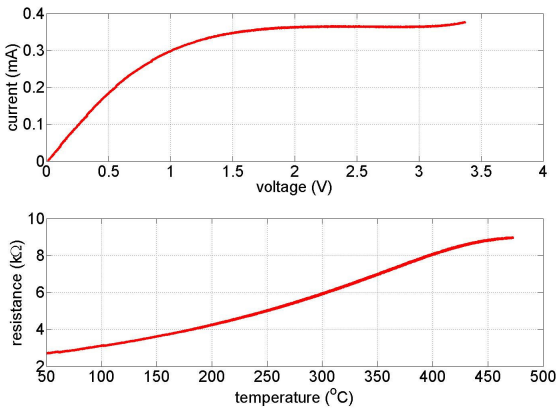

Fig. 6. The static voltage vs. current relationship and resistance vs. temperature relationship ($g(.)$) of the write heater.

First the nonlinear function relating the resistance with the temperature, g, was obtained as described in the preceding section (see Figure 6). Note that $g(.)$ has no dynamics and is valid over all frequencies.

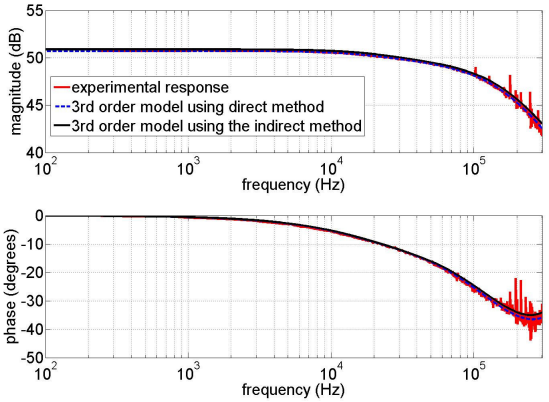

Fig. 7. Experimentally obtained frequency response relating the temperature fluctuations with power fluctuations and the models obtained using the two approaches.

The linear operator $\mathbf{T}_{TP_x}$ was identified next. For this a 50 mV chirp signal offset by 1V was used. The micro-cantilever tip was brought into contact with a polymer medium using a nanopositioner. This would fix the heater-sample separation to be around 500 nm, which is the tip-height of these micro-cantilevers. First $\mathbf{T}_{TP_x}$ was identified using the first approach described in the previous section. A third-order transfer function was found to model the dynamics appropriately and is given by

$$\mathbf{T}_{TP_x}(s) = \frac{1.645 \times 10^{23} s^2 + 5.358 \times 10^{29} s + 5.602 \times 10^{34}}{s^3 + 2.004 \times 1021 s^2 + 1.871 \times 10^{27} s + 1.627 \times 10^{32}}. \quad (6)$$

Then $\mathbf{T}_{TP_x}$ was also identified using the second method. The frequency response of the operator relating the current fluctuations with the voltage fluctuations was obtained. A third-order transfer function was found to model the frequency response adequately and is given by

$$\mathbf{T}_{\tilde{IV}_x}(s) = \frac{0.2043 s^3 + 2.431 \times 10^6 s^2 + 2.262 \times 10^{12} s + 2.933 \times 1017}{s^3 + 9.649 \times 10^6 s^2 + 1.249 \times 10^{13} s + 1.889 \times 10^{18}}.$$

Using Equation (2), the thermal system $\mathbf{T}_{TP_x}$ was derived. From Figure 7 it can be seen that there is excellent agreement between the models of $\mathbf{T}_{TP_x}$ obtained using the two approaches.

3.2 Generation of arbitrary temperature signals

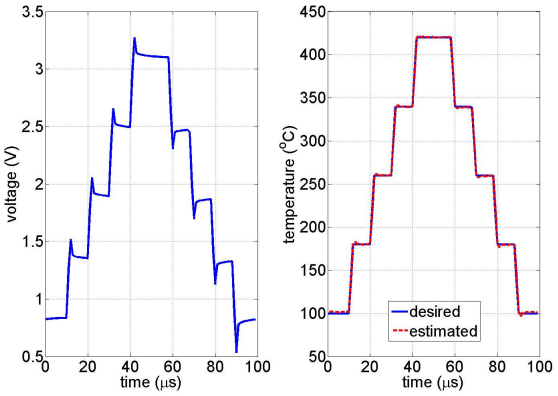

Fig. 8. Generation of arbitrary temperature signals.

A fascinating application of the write heater model is its use to generate voltage signals corresponding to desired temperature signals. Because of the nonlinear electrical feedback and the linear but non-first-order thermal dynamics, it is not straightforward to obtain the voltage signals required for desired temperature signals. However, by separating the nonlinear block from the linear dynamic block, we can systematically arrive at the voltage signals. If $T_{des}(t)$ is the desired temperature signal, then the corresponding resistance signal is given by $R_{des}(t) = g(T_{des}(t))$. Also, the corresponding power profile that generates $T_{des}(t)$ is given by $P_{des}(t) = \mathbf{T}_{TP_x}^{-1}(T_{des}(t))$. Note that $\mathbf{T}_{TP_x}$ has to be inverted, which is achieved by fitting the experimentally obtained frequency response with a minimum phase transfer function and inverting the latter. The required input voltage profile is given by $\sqrt{P_{des}(t)R_{des}(t)}$.

One such experiment was performed using the write heater. The results are presented in Figure 8. The desired temperature signal is shown in Figure 8. The synthesized voltage signal that results in the desired temperature signal is also shown in Figure 8. This voltage signal was applied to the write heater and the resulting resistance signal measured. The temperature signal is estimated from this resistance signal using $g(.)$. There is remarkable agreement between the desired and the estimated temperature signal. Micro-second-scale temperature pulses can be generated using this scheme. Moreover this ability to generate temperature signals of arbitrary shape is a further validation of the modeling approach.

4. THE READ MICRO-HEATER

In this section we present the identification of the read heater. Sensing is facilitated by the variation of the thermal system as a function of the heater-sample or the tip-sample separation. Hence we need to identify $\mathbf{T}_{TP_x}$ as a function of the heater-sample separation. From these measurements, the sensing transfer function $\mathbf{T}_{\tilde{I}\tilde{x}_x}$ can be evaluated. We also discuss the noise sources and the resulting sensor resolution briefly.

4.1 Experimental Identification

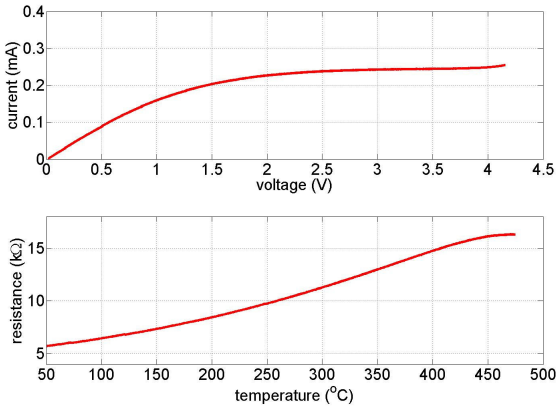

Fig. 9. The static voltage vs. current relationship and resistance vs. temperature relationship ($g(.)$) corresponding to the read heater.

The static relationship between the temperature and resistance was obtained as in the case of the write heater (see Figure 9). Next $\mathbf{T}_{TP_x}$ is identified at various values of tip-sample separation. The thermal system identified when the tip is in contact with the sample (which means a heater-sample separation of ≈ 500 nm) is given by

$$\mathbf{T}_{TP_x}(s) = \frac{378.7}{3\times 10^{-6}s+1}.$$

The significant difference with the write heater is that a first-order model captures the thermal system dynamics, whereas a higher-order transfer function was required to capture the thermal system dynamics in the case of the write transducer.

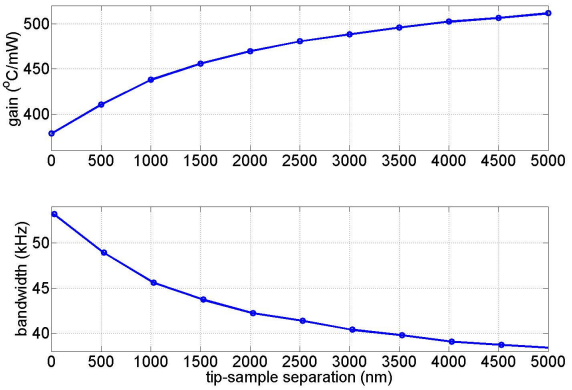

Fig. 10. Variation of the gain and bandwidth of $\mathbf{T}_{TP_x}$ as a function of heater-sample separation.

As the heater-sample separation is increased, intuitively, the linear thermal system should become slower because the conduction path through the air gap between the heater and the substrate is getting longer. Moreover, as the heater is getting thermally more isolated, the heater should heat up to a higher temperature for a given power input. This is precisely what is observed experimentally. The change in the gain and bandwidth is shown in Figure 10.

4.2 Sensing transfer function

To obtain the sensing transfer function the relationship given by Equation (5) is used to derive $\mathbf{T}_{\tilde{I}\tilde{x}_x}$. From the gain variation of the thermal system as a function of heater-sample separation (Figure 10), we obtain $\alpha = K'(x)/K(x)$. Using (5), $\mathbf{T}_{\tilde{I}\tilde{x}_x}$ is evaluated at various heater-sample separations. In particular $\mathbf{T}_{\tilde{I}\tilde{x}_x}$ while the tip is in contact with the sample is given by

$$\mathbf{T}_{\tilde{I}\tilde{x}_x}(s) = \frac{-9.844\times 10^{-6}}{2.281\times 10^{-6}s+1}.$$

Note that Equation (5) is derived with the assumption that the change in the gain of the thermal system is primarily responsible for sensing. However, from Figure 10, we see that there also is a significant change in the bandwidth of the thermal system. A simulation was performed to obtain the sensing transfer function that also accounts for the varying bandwidth of the thermal system besides the varying gain. The resulting sensing transfer function was only marginally different from that obtained using (5). This further confirms the assumption that the gain change of the thermal system is primarily responsible for sensing.

The sensing transfer functions were evaluated at other tip-sample separations and the results are shown in Figure 11. It can be seen that the sensitivity and bandwidth both deteriorate as the heater-sample separation increases. Relation (5) also provides a straightforward means of ascertaining the sensitivity and bandwidth variations as a function of bias voltage or power.

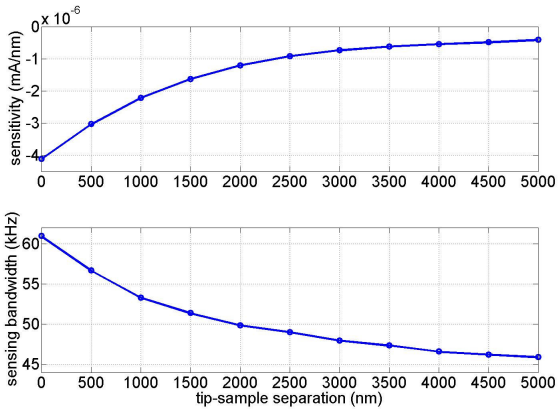

Fig. 11. Variation of the gain and bandwidth of $\mathbf{T}_{\tilde{I}\tilde{x}_x}$ as a function of heater-sample separation.

4.3 Sensing resolution

The predominant noise sources in thermo-electric sensing are the thermal noise of the silicon resistor and $1/f$ noise. The $1/f$ noise contribution is more difficult to predict. This conductance fluctuation noise is typically described by a model developed by Hooge that relates the $1/f$ noise to the number of carriers in the bulk of the resistor and assumes that it is proportional to the dissipated power. Let n_{R_j} represent the thermal noise and let n_{R_f} denote the $1/f$ noise component. Both random processes are thought of as equivalent resistance fluctuations. Let $S_{n_{R_j}}$ be the power spectral function corresponding to n_{R_j} given by

$$S_{n_{R_j}}(f) = \frac{4k_B T_0 R_0^2}{P_0}, \tag{7}$$

where k_B is the Boltzmann constant. Let $S_{n_{R_f}}$ denote the power spectral function corresponding to rn_f given by

$$S_{n_{R_f}}(f) = \frac{\alpha}{fN_{carr}}. \tag{8}$$

where α denotes the Hooge factor and N_{carr} denotes the number of carriers in the bulk of the resistor. The net resistance noise is the sum of these two noise sources given by $n_R = n_{R_j} + n_{R_f}$.

From Figure 5, the resulting current fluctuation corresponding to an input resistance fluctuation is given by

$$\begin{aligned}\tilde{I} &= \frac{-I_0/R_0}{1+I_0^2 g'(T_0)\mathbf{T}_{TP_x}} n_R \\ &= \mathbf{T}_{\tilde{I}n_{Rx}} n_R.\end{aligned}$$

Note that the measured resistance fluctuation is slightly different from the "input" resistance fluctuation given by

$$\tilde{R} = \frac{1}{1+I_0^2 g'(T_0)\mathbf{T}_{TP_x}} n_R. \tag{9}$$

This effective "cooling" is another effect of the inherent electrical feedback.

The signal-to-noise ratio is given by

$$SNR = 20\log\left(\frac{\sqrt{\int_{\mathrm{BW}} |\mathbf{T}_{\tilde{I}\tilde{x}_x}(f)|^2 df}}{\sqrt{\int_{\mathrm{BW}} |\mathbf{T}_{\tilde{I}n_{Rx}}(f)|^2 S_{n_R}(f) df}}\right). \tag{10}$$

For the simulations presented here, the SNR is obtained to be 7.8 dB for a power of 0.159 mW and a bandwidth, BW = 100 kHz. As in the case of sensitivity and bandwidth, relation (5) can be used to obtain the SNR variation as a function of the applied voltage or power.

5. THE THERMAL POSITION SENSORS

The thermal position sensors are relatively large heaters. However, the dynamics are similar to those of the read heaters. Unlike the read heaters, the thermal position sensors are typically operated in a differential configuration. Besides the obvious advantage of having an increased SNR, the differential sensors were observed to be more linear than the individual sensors. This can be explained by the models.

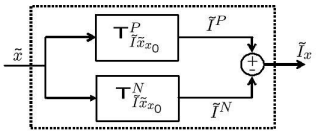

Fig. 12. Differential sensing configuration.

If we assume that each sensor is an operator mapping the scan table motion, $\tilde{x}$, to the corresponding current fluctuation $\tilde{I}$, differential sensing can be viewed as shown in Figure 12. Let us assume that first-order transfer functions capture the two sensing transfer functions corresponding to the positive and negative sensors denoted by

$$\mathbf{T}^P_{\tilde{I}\tilde{x}_x} = \frac{-K_p(x)}{\tau_p(x)s+1} \text{ and}$$
$$\mathbf{T}^N_{\tilde{I}\tilde{x}_x} = \frac{K_n(x)}{\tau_n(x)s+1}.$$

Then the differential sensing transfer function, $\mathbf{T}^{PN}_{\tilde{I}\tilde{x}_x}$, is given by

$$\mathbf{T}^{PN}_{\tilde{I}\tilde{x}_x} = -\frac{[K_p(x)+K_m(x)]\left(\frac{\tau_p(x)K_m(x)+\tau_m(x)K_p(x)}{K_p(x)+K_m(x)}s+1\right)}{(\tau_p(x)s+1)(\tau_m(x)s+1)}. \tag{11}$$

The gain of $\mathbf{T}^{PN}_{\tilde{I}\tilde{x}_x}$ is the sum of the local gains of $\mathbf{T}^P_{\tilde{I}\tilde{x}_x}$ and $\mathbf{T}^N_{\tilde{I}\tilde{x}_x}$. Moreover the newly formed zero cancels out the difference in the pole positions as a function of the scanner position. Hence the differential sensor is much more linear along the travel range of the micro-scanner than an individual sensor.

To identify the sensitivity and sensing bandwidth of the thermal position sensors, we have to identify the sensing transfer functions of the individual positive and negative sensors. As done in the previous section, the thermal systems and the nonlinear temperature-dependent resistance relationships are identified.

The relationship between the current and voltage and the identified temperature-dependent resistance, $g(.)$, for the two thermal position sensors are shown in Figure 13. It can be seen that the resistance values are relatively small compared with the much smaller read and write heaters presented earlier. Moreover, $g(.)$ is much more linear than in other micro-heaters presented so far. The thermal systems $\mathbf{T}_{TP_x}$ corresponding to both the thermal position sensors are identified at different micro-scanner positions, and are well captured by first-order transfer functions at all positions.

There is a large variation in the gain and bandwidth owing to the large motion range of the micro-scanner and the corresponding large change in the overlap. The resulting variation in gain and bandwidth as a function of the micro-scanner position is shown in Figure 14. It can be seen that as the scanner moves from -50 μm to 50 μm, the gain of $\mathbf{T}_{TP_x}$ increases for the positive sensor

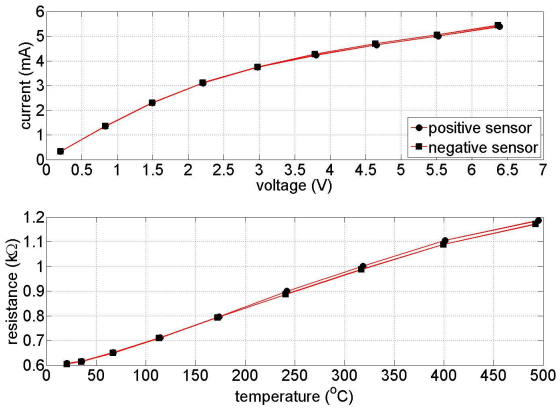

Fig. 13. Static *I-V* curves and the derived temperature-dependent resistance relationships for the positive and negative sensors.

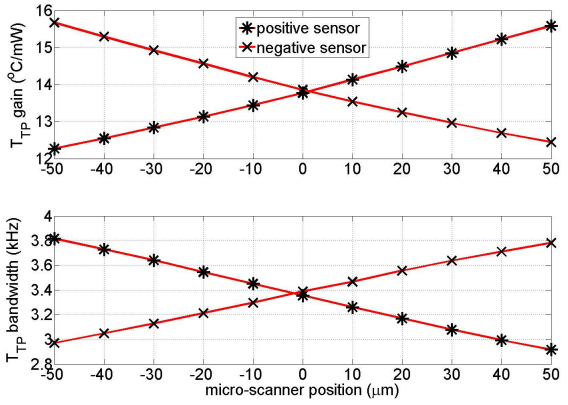

Fig. 14. Gain and bandwidth variations of the thermal systems of the positive and negative sensors as a function of the micro-scanner position.

whereas it reduces for the negative sensor. This is intuitive because, in a differential configuration, as the overlap of one sensor with the scan table reduces, the overlap of the other sensor with the scan table increases.

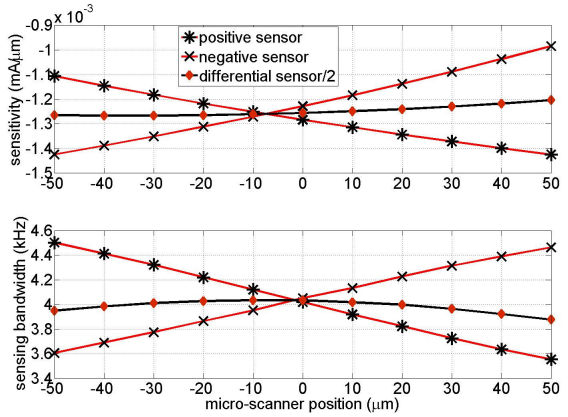

Fig. 15. Sensitivity and sensing bandwidth variations of the positive and negative sensors compared with those of the differential sensor.

Using the relationship given by (5) and the gain variations depicted in Figure 14, the sensing transfer function $\mathbf{T}_{\tilde{I}\tilde{x}_x}$ is obtained for both the positive and negative sensors at different positions of the scanner. Ideally, for a linear sensor across the entire travel range of the scanner, $\mathbf{T}_{\tilde{I}\tilde{x}_x}$ need to be invariant across the entire range. However, for individual thermal position sensors, $\mathbf{T}_{\tilde{I}\tilde{x}_x}$ varies significantly when evaluated at different scanner positions. The differential sensing transfer function is evaluated using the individual sensing transfer functions. The sensitivity and sensing bandwidth variations as a function of the micro-scanner position are shown in Figure 15. Owing to the averaging effect of differential sensing, the differential sensing transfer function is remarkably linear with an average sensitivity of -2.5×10^{-3} mA/μm and bandwidth of 4 kHz.

6. CONCLUSION

Micro-fabricated silicon cantilevers with integrated heating elements find numerous applications in nanoscale science and technology. In the probe-based data-storage effort pioneered by IBM, they serve as writers for thermo-mechanical recording on thin polymer films and readers for thermo-electric topography sensing. They also find application as highly accurate position sensors. There is significant interest in understanding and identifying the dynamics of these micro-heaters. In this article the dynamics of these micro-heaters is viewed from a systems perspective. The micro-heater is thought of as a linear thermal system in feedback with a nonlinear temperature-dependent resistance function. The experimental identification of the various micro-heaters is presented based on this model.

ACKNOWLEDGEMENTS

We would like to thank M. Despont, U. Drechsler, M. Lantz and H. Rothuizen for the design and fabrication of the micro-cantilevers and position sensors used in this work. We would also like to thank P. Bächtold for his help with the electronic circuits. Special thanks go to A. Pantazi, Ch. Hagleitner, U. Dürig, H. Pozidis and E. Eleftheriou for fruitful discussions.

REFERENCES

D. G. Cahill, W. K. Ford, K. E. Goodson, G. D. Mahan, A. Majumdar, H. J. Maris, R. Merlin, and S. R. Phillpot. Nanoscale thermal transport. *Journal of Applied Physics*, 93(2):pp. 793–818, 2003.

U. Dürig. Fundamentals of micro-mechanical thermo-electric sensors. *Journal of Applied Physics*, 98:044906, 2005.

E. Eleftheriou, T. Antonakopoulos, G. K. Binnig, G. Cherubini, M. Despont, A. Dholakia, U. Durig, M. A. Lantz, H. Pozidis, H. E. Rothuizen, and P. Vettiger. Millipede-a MEMS based scanning-probe data storage system. *IEEE Transactions on Magnetics*, 39(2):pp. 938–945, 2003.

M. A. Lantz, G. K. Binnig, M. Despont, and U. Drechsler. A micromechanical thermal displacement sensor with nanometer resolution. *Nanotechnology*, 16:1089–1094, May 2005.

K. Park, J. Lee, Z. M. Zhang, and W. P. King. Frequency-dependent electrical and thermal response of heated atomic force microscope cantilevers. *Journal of Microelectromechanical Systems*, 16(2):213–222, 2007.

H. M. Pollock and A. Hammiche. Micro-thermal analysis: techniques and applications. *J. Phys. D: Appl. Phys.*, 34:pp. R23–R53, 2001.

D. Wiesmann and A. Sebastian. Dynamics of silicon micro-heaters: Modeling and experimental identification. In *Proceedings of the IEEE MEMS Conference*, pages 182–185, February 2006.